Calculation of Magnetically Induced Currents in Hydrocarbon Nanorings

Stefan Taubert,*,† Dage Sundholm,*,† Jonas Jusélius,*,‡ Wim Klopper,*,§ and Heike Fliegl*,||

Department of Chemistry, P.O. Box 55 (A.I. Virtanens plats 1), FIN-00014 University of Helsinki, Finland, Centre for Theoretical and Computational Chemistry, University of Tromsø, N-9037 Tromsø, Norway, Institut für Physikalische Chemie, Universität Karlsruhe (TH), D-76128 Karlsruhe, Germany, and Institut für Nanotechnologie, Forschungszentrum Karlsruhe GmbH, Hermann-von-Helmholtz-Platz 1, D-76344 Eggenstein-Leopoldshafen, Germany

Received: June 10, 2008; Revised Manuscript Received: October 1, 2008

Magnetically induced current densities, nuclear magnetic shieldings, and electric polarizabilities of planar ring-shaped hydrocarbons have been studied at the density-functional theory level using the Becke−Perdew (BP86) functional. The current densities were calculated using the Gauge-Including Magnetically Induced Current (GIMIC) method employing gauge-including atomic orbitals. The GIMIC calculations yield rules to estimate the global and local ring−current strengths as well as the current pathways for the hydrocarbon nanorings. For the overall antiaromatic molecules, aromatic groups such as benzene, naphthalene, anthracene, and pyrene moieties localize the ring current making the global ring currents vanish. The ability of the edge groups to localize the currents is related to the aromatic character of the molecule as a whole. The local ring current prefers to follow the edges of the group. Phenalenyl corner moieties are found to introduce strong global ring currents, whereas with fused benzene and pyrene corner groups the global ring current vanishes. Fused benzene rings in the corner or along the edge of overall antiaromatic molecules sustain local ring currents of about the same size as for a free benzene molecule. For the overall aromatic molecules, the global ring current is split along the bonds of the edge moieties, but the detailed division fulfilling Kirchhoff's current law is not easily predictable and must be calculated for each individual bond. At the phenalenyl corner moieties, the global ring current follows the innermost route isolating the rest of the group from the main delocalization pathway. A hydrocarbon nanoring sustaining strong ring currents should be large and formally aromatic with many and large aromatic moieties along the edges. A clear correlation between the strength of the global ring currents and the size of the electric polarizabilities is obtained. The calculated ^{1}H NMR shieldings of a proton in immediate contact to the global ring current vary between 22 ppm and 67 ppm in the studied molecules. The trend correlates well with the global ring−current strengths, which are in the range of 0−88 nA/T. The ^{13}C NMR shieldings are also sensitive to the strength of the global ring current, but they vary less systematically and are not as good an indicator of the current strength as the hydrogen shieldings.

1. Introduction

The design of molecules with special properties for potential new applications, such as molecular switches or optical devices,[1,2] is a demanding challenge. What kind of molecules should for example be used as building blocks in molecular electronics? How should molecules be designed to efficiently transport electrons along desired routes? To answer these kinds of questions, detailed knowledge about the molecular response to external electric or magnetic fields is essential. Computations of molecular electric and magnetic properties like electric polarizabilities, magnetic shielding functions, magnetic susceptibilities, and magnetically induced ring currents can be employed as a first prescreening test to identifying molecules of potential use in molecular switches and devices. A first step in this research area is to design planar molecules having an extended electron delocalization with the ability to transport currents across or around the molecule. Here, we have chosen a set of 21 hydrocarbon molecules fulfilling in this context three important conditions: they are ring shaped, electron rich, and planar. The planarity and ring shape make it more convenient to place them in future applications on a surface. The requirement of electron richness should imply good current transport properties. In the present molecules, this condition is fulfilled by using molecules with potentially highly delocalized π systems. The molecules are constructed using benzene rings and acetylene units as basic building blocks.

The electron delocalization in ring-shaped molecules and the molecular aromaticity are related.[3] The ability to sustain a ring current in an external magnetic field is used as an aromaticity criterion.[4] Hydrocarbons are generally considered to be aromatic when the number of π electrons fulfills Hückel's $(4n + 2)$ rule, with $n = 0, 1, 2, ...$ Antiaromaticity is considered when the π system consists of $4n$ π electrons, with $n = 1, 2, 3, ...$[5] However, the Hückel rule provides little information about the absolute or relative degree of aromaticity. For more extended cyclic hydrocarbons with multiple fused or connected molecular rings, it is less obvious to judge how the π electrons actually participate in the aromatic pathway and contribute to the molecular aromaticity. All π electrons can be involved in the molecular aromaticity. The electron delocalization can also be split into several subunits, that is, separated molecular fragments can be

* Corresponding authors: Stefan.Taubert@helsinki.fi, Dage.Sundholm@helsinki.fi, Jonas.Juselius@chem.uit.no, klopper@chem-bio.unikarlsruhe.de, Heike.Fliegl@int.fzk.de.
† University of Helsinki.
‡ University of Tromsø.
§ Universität Karlsruhe.
|| Forschungszentrum Karlsruhe GmbH.

10.1021/jp805086q CCC: $40.75
Published on Web 12/04/2008

aromatic in the sense that they sustain ring currents in the presence of an external magnetic field, but the aromatic pathways are independent; no electron delocalization pathways exist between the subunits. The situation can be even more complicated, since the delocalization pathways can consist of several connected routes or they can be considered to consist of a superposition of several pathways.

We adopt here the magnetic criterion for the definition of aromaticity and electron delocalization, that is, the strength of the magnetically induced current (actually the size of the ring current susceptibility at zero magnetic field) passing chemical bonds or circling around the molecular rings. If the magnetic response due to the ring current is of diamagnetic character, the molecule is considered aromatic, whereas a paramagnetic response characterizes antiaromatic molecules. If the molecule exposed to an external magnetic field does not sustain a ring current, or if the ring currents are very weak, the molecule is nonaromatic. The explicit values for the strength of the magnetically induced currents can be obtained by numerical integration of the current density passing given chemical bonds.[6] The aromatic ring−current shielding (ARCS)[7−10] and nucleus-independent chemical shift (NICS) calculations[4,11−14] provide indirect measures of the current strengths. For complex molecules, it is often difficult to assess the degree of aromaticity based on magnetic shielding functions. The magnetically induced current densities can be explicitly calculated at ab initio levels of theory.[6,15−18] The magnetic character of the molecules can be obtained from plots of the spatial distribution of the current densities.[16,17,19,20] The graphs can convey information about the current pathways and strength, but a more detailed representation can be obtained by complementing the maps with numerical integration of the current density passing through selected chemical bonds.[6]

In this work, we have used the gauge-including magnetically induced current (GIMIC) method[6] to determine the strengths of the magnetically induced currents circling the molecular rings of the planar hydrocarbons. The GIMIC method employs gauge-including atomic orbitals (GIAO)[21−24] to improve basis set convergence of the current density and to reduce the errors due to lack of true gauge invariance.[25] The ring−current susceptibilities for the main molecular ring is used to quantify the electron delocalization of the hydrocarbons. Calculated current pathways and strengths have previously been used to characterize the aromaticity of metal clusters, fullerenes, and complex multiring molecules.[6,26−31] An alternative approach also used here to assess electron delocalization effects is to calculate the polarizability tensor, since the polarizability measures how easily the electron density is deformed by an applied electric field. Studies on the polarizability of aromatic systems have shown the π -polarizability to be merely a qualitative descriptor of aromaticity of similar systems.[32,33] The ^{1}H NMR and ^{13}C NMR shieldings are also reported because especially ^{1}H NMR shieldings are known to be strongly affected by ring currents.[13]

2. Theory

2.1. Current Densities. In the presence of a uniform, time-independent magnetic field with a flux **B**, a current density $\mathbf{J}^{\mathbf{B}}(\mathbf{r})$ is induced within the molecular electron density:

$$\mathbf{J}^{\mathbf{B}}(\mathbf{r}) = \frac{i}{2}\int \mathrm{d}\mathbf{r}_2, ..., \mathrm{d}\mathbf{r}_n(\Psi * \nabla\Psi - \Psi\nabla\Psi * + 2i\mathbf{A}\Psi * \Psi) \tag{1}$$

where Ψ is the wave function and **A** is the vector potential describing both the external magnetic field and the magnetic fields arising from the nuclei. The second-order interaction energy due to the interaction of nuclear magnetic moments with an external magnetic field can be given in terms of the current density and the vector potential due to the corresponding nuclear magnetic moment[17]

$$E^{mB} = -\int \mathbf{A}_{\mathbf{I}}{}^{m}(\mathbf{r}) \cdot \mathbf{J}^{\mathbf{B}}(\mathbf{r})\, \mathrm{d}\mathbf{r} \tag{2}$$

The nuclear magnetic shielding tensor can be obtained by differentiating the total energy with respect to the nuclear magnetic moments and the components of the external magnetic field in the limit of zero magnetic field as

$$\sigma^{I}_{\alpha\beta} = \frac{\partial^2 E}{\partial m_\alpha{}^{I}\, \partial B_\beta}{}^{\mathbf{B}=0}_{\mathbf{m}_I=0} \tag{3}$$

Evaluation of the second derivative in eq 3 using eq 2 yields the following expression for the nuclear magnetic shielding tensor[17]

$$\sigma^{I}_{\alpha\beta} = -\epsilon_{\alpha\delta\gamma}\int \frac{(r_\delta - R_{I\delta})}{|\mathbf{r} - \mathbf{R}_I|^3}\mathscr{T}_\gamma^{B_\beta}\, \mathrm{d}\mathbf{r} \tag{4}$$

where

$$\mathscr{T}_\gamma^{B_\beta}(\mathbf{r}) = \frac{\partial J_\gamma(\mathbf{r})}{\partial B_\beta} \tag{5}$$

are the tensor elements of the first-order-induced current density and $\epsilon_{\alpha\delta\gamma}$ is the Levi−Civita tensor.

The electronic energy of a molecular system can generally be written in terms of the one-electron ($D_{\mu\nu}$) and two-electron ($d_{\mu\sigma\nu\rho}$) density matrices in the atomic-orbital (AO) representation contracted with the corresponding Hamiltonian matrix elements. The derivative-theory-based expression for calculating magnetic shielding tensor elements is[34]

$$\sigma^{I}_{\alpha\beta} = \sum_{\mu\nu} D_{\mu\nu}\frac{\partial^2 h_{\mu\nu}}{\partial m_\alpha{}^{I}\, \partial B_\beta} + \sum_{\mu\nu}\frac{\partial D_{\mu\nu}}{\partial B_\beta}\frac{\partial h_{\mu\nu}}{\partial m_\alpha{}^{I}} \tag{6}$$

where $\partial D_{\mu\nu}/\partial B_\beta$ are the magnetically perturbed density matrices and $\partial h_{\mu\nu}/\partial m_\alpha{}^I$ and $\partial^2 h_{\mu\nu}/\partial m_\alpha{}^I \partial B_\beta$ are the corresponding derivatives of the Hamiltonian integrals in the AO representation. Equating eqs 6 and 4 and explicitly introducing the one-electron basis functions, we obtain an equation that relates nuclear magnetic shielding and the current-density tensors. By introducing GIAOs, the working equations for the calculation of the various components of the magnetically induced current-density tensor, $\mathscr{T}_\alpha^{B_\beta}(r)$ becomes

$$\mathscr{T}_\alpha^{B_\beta}(\mathbf{r}) = \sum_{\mu\nu} D_{\mu\nu}\frac{\partial \chi_\mu{}^*(\mathbf{r})}{\partial B_\beta}\frac{\partial \tilde{h}}{\partial m_\alpha{}^{I}}\chi_\nu(\mathbf{r}) + \sum_{\mu\nu} D_{\mu\nu}\chi_\mu{}^*(\mathbf{r})\frac{\partial \tilde{h}}{\partial m_\alpha{}^{I}}\frac{\partial \chi_\nu(\mathbf{r})}{\partial B_\beta} + \sum_{\mu\nu}\frac{\partial D_{\mu\nu}}{\partial B_\beta}\chi_\mu{}^*(\mathbf{r})\frac{\partial \tilde{h}}{\partial m_\alpha{}^{I}}\chi_\nu(\mathbf{r}) - \epsilon_{\alpha\beta\delta}\left[\sum_{\mu\nu} D_{\mu\nu}\chi_\mu{}^*(\mathbf{r})\frac{\partial^2 \tilde{h}}{\partial m_\alpha{}^{I}\, \partial B_\delta}\chi_\nu(\mathbf{r})\right] \tag{7}$$

The common denominator $|\mathbf{r} - \mathbf{R}_I|^3$ has been removed for the operators $\partial\tilde{h}/\partial m_\alpha{}^I$ and $\partial^2\tilde{h}/\partial m_\alpha{}^I\partial B_\delta$. The expression in eq 7 is easily evaluated at any point in space, since it only involves basis-function values and values of the derivatives of basis functions at the grid points combined with the appropriate one-electron density matrix elements. The explicit dependence of each individual contribution on the nuclear position $\mathbf{R}_I$ cancels

out in the sum of all contributions, making the current-density tensor independent of the nuclear positions $\mathbf{R}_I$ and the magnetic moments m_α^I, as it should be.

A vector expression for the calculation of the current density in each grid point can be written as

$$\mathscr{I}_\alpha^{B_\beta} = \mathbf{v}^T\mathbf{P}_\beta\mathbf{d}_\alpha - \mathbf{b}_\beta{}^T\mathbf{D}\mathbf{d}_\alpha + \mathrm{v}^T\mathbf{D}\mathbf{q}_{\alpha\beta} - \epsilon_{\alpha\beta\gamma}\frac{1}{2}(\mathbf{v}^T\mathbf{D}\mathbf{v})\mathbf{r}_\gamma \quad (8)$$

where $\mathbf{D}$ is the AO density matrix, $\mathbf{P}_\alpha$ are the perturbed AO density matrices, and $\mathbf{v}$ is a vector containing the basis function values in each grid point $\mathbf{r}$. The vectors $\mathbf{b}_\alpha$, $\mathbf{d}_\alpha$, and $\mathbf{q}_{\alpha\beta}$ are given by

$$\mathbf{b}_\alpha = \frac{\partial \mathbf{v}}{\partial \mathbf{B}_\alpha}; \qquad \mathbf{d}_\alpha = \frac{\partial \mathbf{v}}{\partial \mathbf{r}_\alpha}; \quad (9)$$

$$\mathbf{q}_{\alpha\beta} = \frac{\partial^2 \mathbf{v}}{\partial \mathbf{r}_\alpha \mathbf{B}_\beta} \qquad (\alpha, \beta \in x, y, z)$$

The density matrices $\mathbf{D}$ and $\mathbf{P}_\alpha$ are obtained from standard ab initio program packages capable of calculating nuclear magnetic shielding tensors.

2.2. Polarizabilities. Polarizabilities can be obtained perturbatively as the second derivative of the ground-state energy with respect to an applied external electric field. In the ESCF module[35−38] of the TURBOMOLE package,[39] the dynamic polarizability tensor $\alpha_{\alpha\beta}(\omega)$; $\alpha, \beta \in x, y, z$ is calculated at frequency ω within the time-dependent density-functional theory (TDDFT) framework[37] as

$$\alpha_{\alpha\beta}(\omega) = \langle \mu_\alpha | (\mathbf{\Lambda} - \omega\mathbf{\Delta})^{-1} | \mu_\beta \rangle \quad (10)$$

where μ denotes matrix elements over the electric dipole moment operator. The matrices $\mathbf{\Lambda}$ and $\mathbf{\Delta}$ are defined as

$$\mathbf{\Lambda} = \begin{pmatrix} \mathbf{A} & \mathbf{B} \\ \mathbf{B} & \mathbf{A} \end{pmatrix}, \qquad \mathbf{\Delta} = \begin{pmatrix} 1 & 0 \\ 0 & -1 \end{pmatrix} \quad (11)$$

Definitions of the $\mathbf{A}$ and $\mathbf{B}$ matrices and a thorough interpretation of the $\mathbf{\Lambda}$ and $\mathbf{\Delta}$ matrices are given for example in ref 37. One denotes the unit matrix. The static polarizability is obtained when ω in eq 10 is set to zero. Because the studied molecules are planar and possessing D_{6h} or D_{3h} symmetry, only the α_{xx}, α_{yy}, and α_{zz} components are nonzero and $\alpha_{xx} = \alpha_{yy}$ holds. The polarizability anisotropy $\mathbf{A}$ is calculated as

$$A = \sqrt{\frac{3}{2}\left|(\alpha_{xx}{}^2 + \alpha_{yy}{}^2 + \alpha_{zz}{}^2) - \frac{1}{3}(\alpha_{xx} + \alpha_{yy} + \alpha_{zz})^2\right|} \quad (12)$$

3. Computational Details

The TURBOMOLE program package[39] has been used in all calculations except for calculating the current densities. They were obtained with GIMIC,[6] which is a separate program interfaced to TURBOMOLE. The molecular structures were optimized at the density-functional theory (DFT) level using the gradient corrected Becke−Perdew (BP86) functional,[40−42] the RI-J technique,[43] and the new Karlsruhe split-valence quality basis sets augmented with polarization functions (def2-SVP).[44] All structures are available in Supporting Information.

Static polarizabilities and nuclear magnetic shieldings were calculated at the BP86 level using the same basis sets. In the magnetic shielding calculations, gauge-including atomic orbitals (GIAO) were employed.[24,45] The magnetically induced current densities were deduced from the one-particle density matrix and the magnetically perturbed density matrices calculated at the BP86 level using the Gauge-Including Magnetically Induced Current (GIMIC) approach.[6] A quantitative measure of the electron delocalization around the molecular rings was obtained from the current densities. The current-density tensor is independent of the direction of the magnetic field, whereas the contraction of the tensor with an explicit magnetic field makes the induced current density direction dependent. The diamagnetic and paramagnetic contributions to the ring−current susceptibilities were determined by numerical integration of the current density passing through cut planes perpendicular to selected bonds of the molecular rings. The current density was calculated in discrete grid points in the cut plane and integrated numerically. The cut planes for the main molecular rings extend 10 bohr inward and outward, as well as upward and downward, from the chosen C−C bond. The width of the plane is in some cases smaller to avoid that it crosses the center of a benzene ring and thereby double-counting some current density, while the height of the plane is 10 bohr in all calculations.

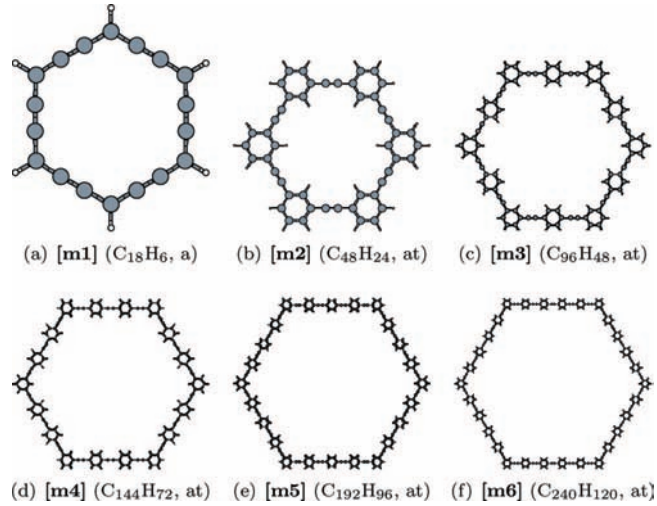

Figure 1. The first series of molecules consisting of fused benzene rings in the molecular macrocycle. The used abbreviations, the chemical brutto formula, and the expected aromaticity according to Hückel's rule is given (a = aromatic, at = antiaromatic).

4. The Investigated Molecules and Used Nomenclature

The investigated hydrocarbon nanorings form large hexagons whose edges are built of carbon atoms linked to each other with alternating single and triple bonds. The molecules denoted [**m1**]−[**m21**] are shown in Figures 1−4. Benzene, naphthalene, and anthracene moieties are attached to the carbon chain along the edges of the hexagons. The corners consist of benzene, phenalenyl, or pyrene groups. The investigated molecules have only one kind of corner groups, whereas two different kinds of edge groups can be in the same molecule. The corner groups of [**m1**] are single hydrogen atoms. In Figures 1−4, the aromatic character of the different molecules, assigned according to Hückels rule, is also given.

The number of π electrons contributing to the delocalized π system is equal to the number of carbon atoms. Triple bonds are treated as double bonds, since only two of the electrons can spatially contribute to the delocalized π system. Benzene, naphthalene, anthracene, and pyrene rings contribute each with 6, 10, 14, and 16 π electrons. The CH corner group of [**m1**] forms a radical and contributes with one π electron to the ring system. The phenalenyl corner group of [**m7**] has a radical character and contributes to the π system with 13 electrons.

The ring current circling around the large hexagon is referred to as the *global current*, while the term *local current* refers to

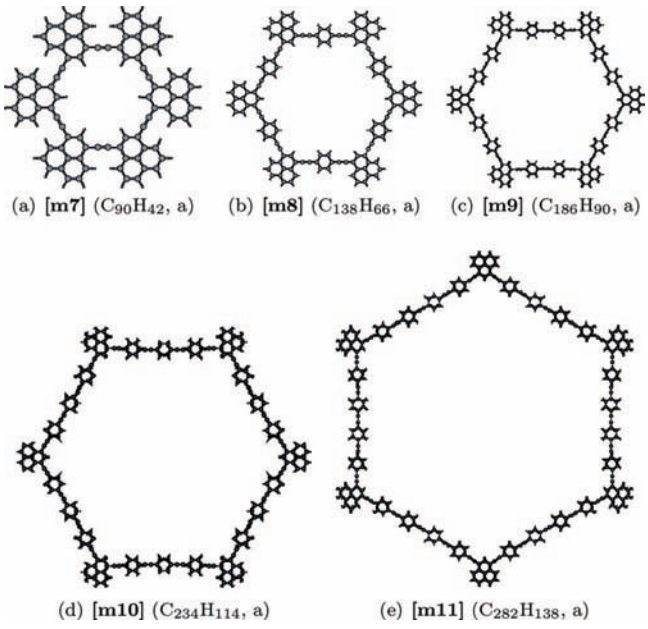

Figure 2. The second series of molecules consisting of six fused phenalenyl groups in the corners of the macroring and fused benzene rings along the edges of the molecular macrocycle. The used abbreviations, the chemical brutto formula, and the expected aromaticity according to Hückel's rule is given (a = aromatic, at = antiaromatic).

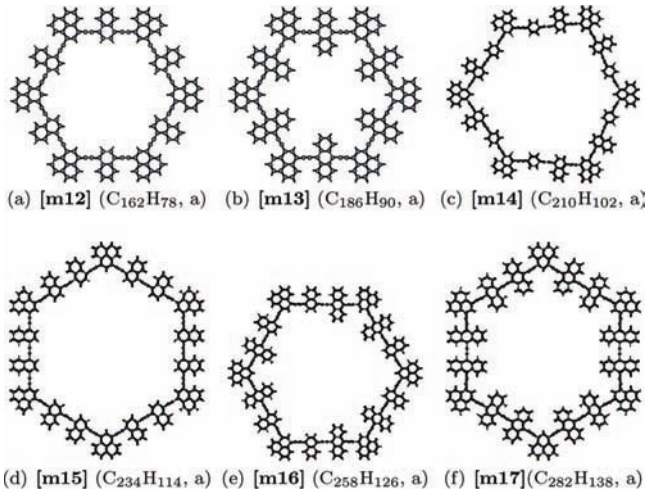

Figure 3. The third series of molecules consisting of six fused phenalenyl groups in the corners of the macroring and fused benzene, naphthalene, and anthracene groups along the edges of the molecular macrocycle. The used abbreviations, the chemical brutto formula, and the expected aromaticity according to Hückel's rule is given (a = aromatic, at = antiaromatic).

the ring currents localized in the side or corner groups or the current passing some part of the edge and corner moieties.

5. Results and Discussion

5.1. Current Densities. The integrated global ring currents for the studied molecules are summarized in Figure 5. The calculations of the magnetically induced current densities of the four series of molecules are discussed in the following sections.

5.1.1. Molecules with Benzenes in the Corners. The starting point for this study is molecule [**m1**] ($C_{18}H_6$) which is a hexagonal ring with conjugated single and multiple bonds. It can be considered as a benzene molecule with C_2 groups fused to the six edges. The π current density of this structure has recently been investigated.[46] All the studied molecules consist of a main hexagonal ring of either D_{6h} or D_{3h} symmetry.

TABLE 1: The Calculated Ring-Current Strengths (nA/T) in the Main Molecular Ring of the First Series of Molecules Labeled [m1] to [m6]

molecule	diamagnetic	paramagnetic	total
[**m1**]	37.48	−4.49	32.99
[**m2**]	9.63	−9.44	0.19
[**m3**]	9.48	−9.58	−0.09
[**m4**]	9.60	−9.44	0.17
[**m5**]	9.48	−9.59	−0.11
[**m6**]	9.80	−9.59	−0.21

The calculation of the magnetically induced ring−current susceptibility (in the following ring current is used for this quantity) for [**m1**] yielded a value of 33.0 nA/T which is about three times the benzene value. It is according to the magnetic ring−current criterion a strongly aromatic molecule. The 18 π electrons are delocalized around the entire ring sustaining the current.

The molecular structure of [**m2**] ($C_{48}H_{24}$), which is the next molecule in this series, is obtained by replacing the six CH groups in the ring corners of [**m1**] by 1,3-fused benzene rings. Calculation of the ring current for the main molecular ring of [**m2**] yielded a very small value of 0.2 nA/T. Thus, no current is sustained in the molecular macroring. The benzenes in the ring corners are instead aromatic sustaining local currents of roughly 9 nA/T. All benzene moieties of this series of molecules ([**m2**]−[**m6**]) have approximately the same current strength. The ring−current strength obtained for a single benzene molecule is 11.6 nA/T at the same level of theory.

The structure of [**m3**] ($C_{96}H_{48}$) can be obtained by inserting six benzene rings with an ethyne substituent into each edge segment of [**m2**]. The edge benzenes are fused to the macroring in the 1,4 positions. The current calculation yielded a tiny global ring current of −0.09 nA/T for the formally antiaromatic [**m3**]. The three largest molecules in this series are also formally antiaromatic. The molecular structures of [**m4**] ($C_{144}H_{72}$), [**m5**] ($C_{192}H_{96}$), and [**m6**] ($C_{240}H_{120}$) were obtained by inserting one, two, and three ethyne-substituted benzene groups to the six edge segments of [**m3**]. The current calculations yielded global ring−current strengths of 0.0−0.2 nA/T for them, because the diamagnetic and paramagnetic ring−current contributions of ±9.5−9.7 nA/T cancel. The formally antiaromatic [**m2**] (48 π electrons), [**m3**] (96 π), [**m4**] (144 π), [**m5**] (192 π), and [**m6**] (240 π) are globally nonaromatic with aromatic benzene rings in the corners and along the edges of the main molecular ring. Table 1 summarizes the calculated global ring currents in the first series of molecules shown in Figure 1. The formally aromatic [**m1**] is shown to be a strongly aromatic molecule using the ring−current criterion. The formally antiaromatic molecules sustain no global ring current, whereas local aromatic ring currents circle around the fused benzene rings.

5.1.2. Molecules with Phenalenyl Corner Groups. The next two series of molecules have [**m7**] ($C_{90}H_{42}$) as starting point. The molecular structure of [**m7**] can be constructed by fusing a naphthalene group to the benzene rings in the corners of [**m2**]. The radical character of the phenalenyl corner groups with formally 13 π electrons promotes the aromatic character of [**m7**] and its analogues shown in Figure 2. The molecular structures of the [**m7**] analogues [**m8**]−[**m11**] were obtained by adding one or several ethyne-substituted benzene groups to the edges of [**m7**]. The π electron count indicates that [**m7**]−[**m11**] should be aromatic, which is also supported by the obtained values for

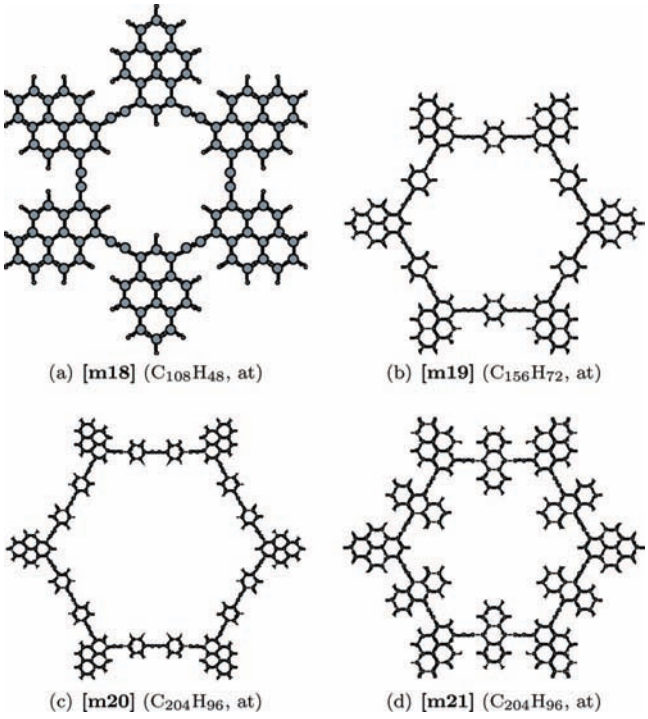

Figure 4. The fourth series of molecules consisting of six fused pyrene groups in the corners of the macroring and fused benzene or anthracene groups along the edges of the molecular macrocycle. The used abbreviations, the chemical brutto formula, and the expected aromaticity according to Hückel's rule is given (a = aromatic, at = antiaromatic).

the global ring−current strengths. Each corner group donates three π electrons to the macroring and the 10 remaining π electrons form an aromatic naphthalene group. The current paths stabilize these parts of the molecule. The magnetic field induces a ring current of 24.5 nA/T in the conjugated 30 π-electron pathway of the innermost molecular ring of [**m7**]. An unconnected ring current of 6.1 nA/T is sustained in the fused naphthalene units, which can be compared to the ring−current strength of 12.7 nA/T for an isolated naphthalene molecule. The current paths are decoupled in the sense that hardly any current passes from the main ring to the naphthalene groups. The ring current of the naphthalene moiety follows the edges of the group, and no current passes through the midbond. For the larger molecules, the naphthalene moiety becomes less aromatic. The local ring current is about half the [**m7**] value for [**m8**]−[**m13**] and it is even less than 1 nA/T for [**m14**]−[**m17**]. The strengths of the current passing selected bonds of the phenalenyl corner groups of [**m7**] are summarized in Table 2 and shown in Figure 6.

The calculated global ring−current strengths for [**m7**]−[**m11**] given in Table 3 show that the addition of one ethyne-substituted benzene group to each edge of the main molecular ring increases the current by more than a factor of 2. The addition of a second benzene group to each edge has little effect on the current strength, whereas the third and the fourth set of benzene groups reduces the current strength by about 10 nA/T each. The descent of the current strength indicates a decrease in the global electron delocalization for the largest members of the series. It can be speculated that the fused benzene rings along the edges do not contribute with enough electrons to maintain the current over long distances. Replacing the benzene rings by anthracene units could maintain the trend of increasing current strength.

Molecules [**m12**]−[**m17**] forming the third series of molecules are shown in Figure 3. They have phenalenyl corner

TABLE 2: The Strength of the Calculated Global Ring Current (in nA/T) of [m7] and [m18] Are Compared to the Local Currents Passing Selected Bonds of the Corner Moieties[d]

cross section	diamagnetic	paramagnetic	total
main ring [**m7**]	29.98	−5.53	24.45
outer route[a] [**m7**]	12.54	−6.48	6.07
midbond[b] [**m7**]	8.02	−8.02	0.00
inner route[c] [**m7**]	28.51	−3.55	24.95
main ring [**m18**]	10.15	−9.80	0.35
outer route[a] [**m18**]	19.34	−4.62	14.72
midbond[b][**m18**]	8.89	−8, 89	0.00
inner route[c] [**m18**]	17.50	−4.62	12.87

[a] The outer route around the corner group. [b] The midbond of the corner group. [c] The innermost route at the corner group. [d] See also Figures 6 and 8.

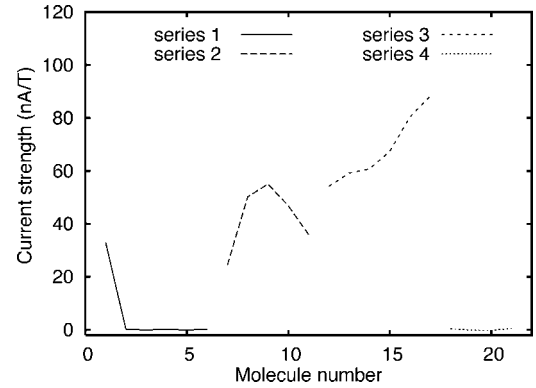

Figure 5. Calculated ring−current strengths (in nA/T) for the studied molecules.

moieties and differ from [**m7**]−[**m11**] series by having naphthalene and anthracene moieties fused to the ring edges. The structure of [**m12**] can be constructed from [**m8**] by fusing a benzene ring to the outer bond of the edge benzene. The structure of [**m13**] differs from that of [**m12**] by having an anthracene group instead of a naphthalene group fused across the ring edges. The [**m14**] structures can be constructed by fusing six benzene rings to one of the fused benzenes on each edges of [**m9**]. The [**m15**], [**m16**], and [**m17**] molecules can analogously be obtained by successively fusing six benzenes to the edge moieties.

The global ring current in [**m12**] is about as strong as that for [**m9**]. Both molecules have 12 benzene rings fused to the edges suggesting that the number of fused benzene moieties to the edges is more important for obtaining hydrocarbon nanorings sustaining strong global ring currents than to increase the size of the nanoring. Actually, the global ring currents are smaller for the largest hydrocarbon nanorings ([**m10**] and [**m11**]) than for [**m13**] and [**m14**]. [**m13**] and [**m14**] have the same number of edge benzenes and the strengths of the global ring currents are also about the same. In the [**m9**], [**m14**]−[**m17**] series of molecules, the global ring current increases by about 6−13 nA/T for each set of six benzene rings fused to the edges. The current strengths obtained for [**m12**]−[**m17**] are summarized in Table 3.

The bonds connecting the aromatic pathways are destabilized resulting in exceptionally long formal aromatic C−C bonds of 1.47 Å for [**m7**]. The bond lengths of the bonds sustaining ring currents are 1.39−1.43 Å. The long C−C bonds between the

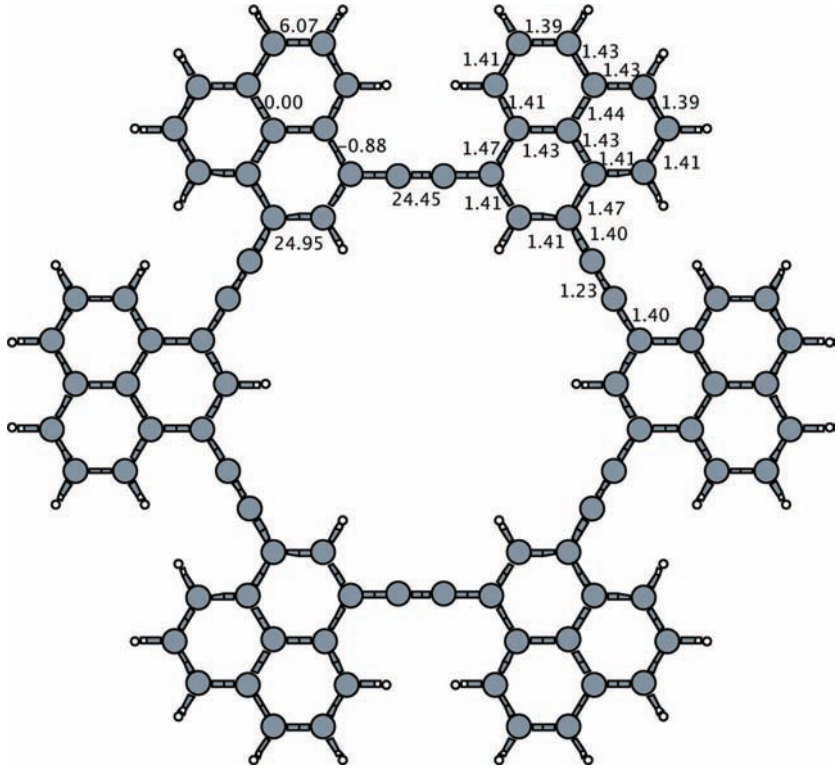

Figure 6. The integrated currents passing selected bonds of the molecule [**m7**] are given in the upper left part of the molecule and the bond lengths in angstroms are shown in the upper right part of the molecule.

TABLE 3: The Integrated Diamagnetic and the Paramagnetic Contributions to the Global Ring Currents (nA/T) of the Investigated Molecules Labeled [m 7] to [m 21]

molecule	diamagnetic	paramagnetic	total
[**m7**]	29.98	−5.53	24.45
[**m8**]	54.10	−3.91	50.19
[**m9**]	58.83	−3.78	55.05
[**m10**]	50.75	−3.95	46.80
[**m11**]	40.38	−4.40	35.98
[**m12**]	58.26	−4.10	54.15
[**m13**]	63.37	−4.18	59.19
[**m14**]	64.47	−3.71	60.76
[**m15**]	71.08	−3.70	67.38
[**m16**]	83.90	−3.52	80.38
[**m17**]	91.93	−3.63	88.31
[**m18**]	10.15	−9.80	0.35
[**m19**]	9.25	−9.42	−0.17
[**m20**]	9.38	−9.66	−0.28
[**m21**]	10.35	−9.88	0.47

outer naphthalene part of the phenalenyl moiety in [**m7**]−[**m17**] also imply that the electron delocalization is decoupled from the inner route of the fused corner benzene ring.

The current calculations on [**m7**]−[**m17**] show that the fused benzene, naphthalene, and anthracene groups along the edges of the molecules host very weak localized ring currents. Addition of the current contributions through each pathway of the fused edge groups yields in all these molecules approximately the global ring current, that is, the fused groups function as junctions fulfilling Kirchhoff's current law. The naphthalene group at the edge of [**m12**] is a typical junction-like group in the aromatic hydrocarbon nanoring with phenalenyl moieties in the corners. The major part of the current follows the innermost (26.2 nA/T) and the outermost (17.3 nA/T) routes of the naphthalene moiety, whereas a smaller part of the current (7.6 nA/T) passes through the middle bond. By adding the current strengths passing the naphthalene moiety, one obtains 51.8 nA/T as compared to the integrated global ring current of 54.2 nA/T. The deviation of 2.4 nA/T (4.5%) can be explained by a slight overestimation of the global current caused by current leakage from the fused naphthalene groups due to the use of finite basis sets. The calculated current can be expected to be somewhat divergent because gauge invariance and charge conservation are obtained only in the limit of complete basis sets.[6,25] The current strengths passing selected bonds in [**m16**] are shown in Figure 7.

5.1.3. Molecules with Pyrene as Corner Groups. The structure of [**m18**] ($C_{108}H_{48}$) can be constructed from **[m2]** by replacing the fused corner benzene by pyrene which has 16 π electrons. The structures of the fourth series of molecules ([**m18**]−[**m21**]) can be derived from that of [**m18**]. The molecular structures of [**m19**] and [**m20**] are obtained by fusing one and two ethyne-substituted benzene groups to the edges of the [**m18**] ring. [**m21**] has an ethyne-substituted anthracene fused to the edges of [**m18**]. The molecular structures are shown in Figure 4. For [**m18**], a strong local ring current of 14.7 nA/T is induced in the corner pyrene groups, whereas a weak global ring current of 0.4 nA/T is sustained by the main molecular ring. According to the calculations of the current density, [**m18**] can be considered to consist of six aromatic pyrene moieties connected by ethyne groups forming a ring. The ring current of the pyrenes circles at the edge, whereas the two carbons in the pyrene center do not participate in the electron delocalization and the current pathway. See Figure 8. When the center carbons are inactive, the corner pyrene becomes according the Hückel's rule an aromatic group with 14 π electrons. The formal π electron count suggests that [**m18**]−[**m21**] are antiaromatic. Table 2 and Figure 8 summarize the current strengths passing selected bonds of the pyrene corner groups of [**m18**]. The global ring current almost vanishes also in [**m19**]]−[**m21**]. The calculated global ring currents of [**m18**]−[**m21**] are compared in Table 3.

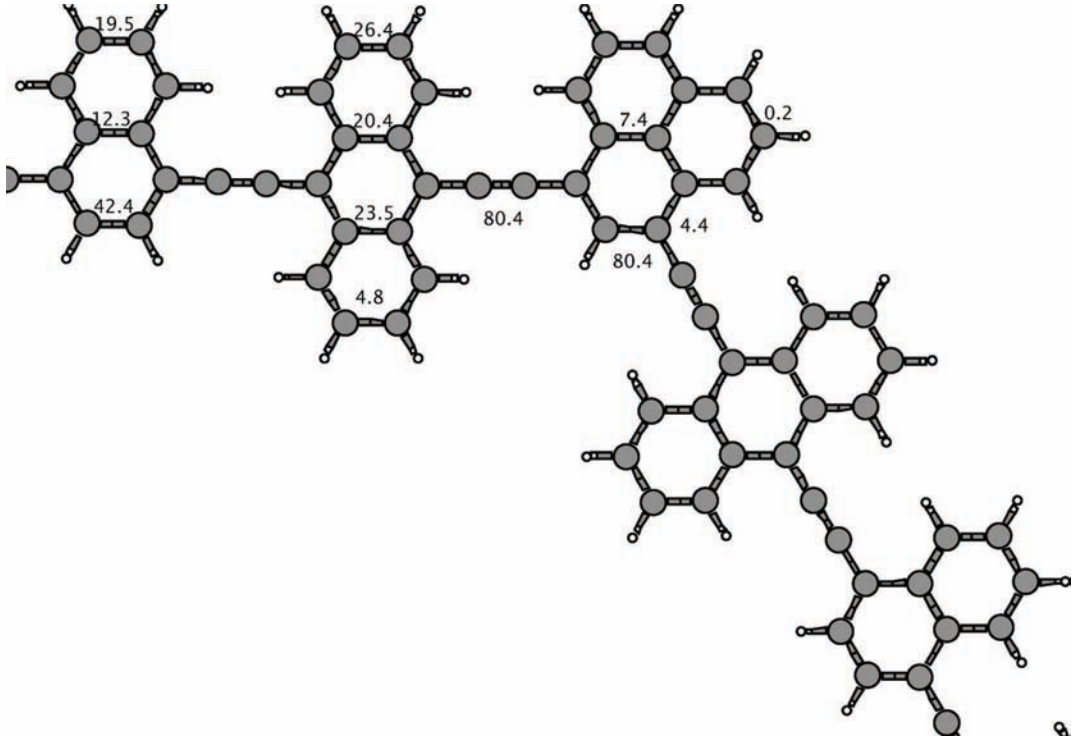

Figure 7. The integrated current strengths passing selected bonds of the corner and edge moieties of [**m16**].

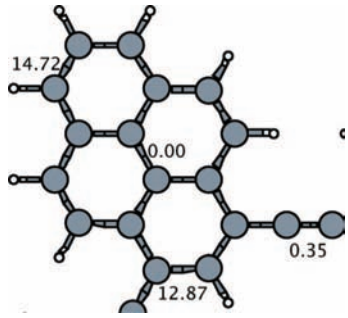

Figure 8. The integrated current strengths passing selected bonds of the corner moiety of [**m18**].

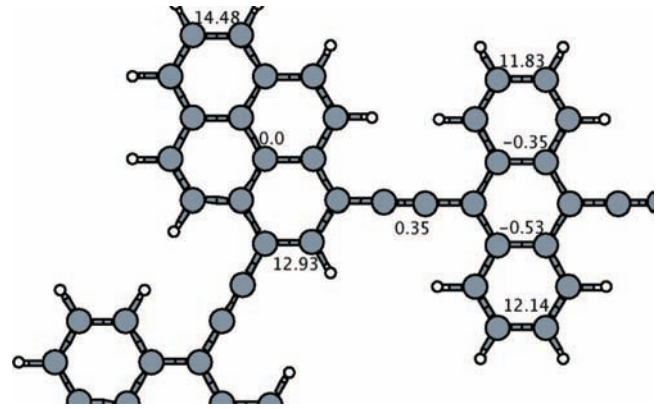

Figure 9. Integrated total currents in the upper left part of the molecule molecule [**m21**].

The calculations show that the edge benzene moieties sustain their own local ring currents, the strengths of which are 7.5−10.4 nA/T. The ring−current strength for the fused benzenes of [**m19**] and [**m20**] is only slightly smaller than the ring−current strength of an isolated benzene molecule indicating that the electron delocalization in the fused benzene is not much affected by the rest of the molecule.

In [**m21**], the pyrene corner moiety and the anthracene moieties at the edges sustain local ring currents. In the anthracenes, the current flows along the outer edges, whereas almost no current (0.5 nA/T) passes through the two bonds in the middle of the anthracene moiety. The local ring−current strength is 11.8 nA/T along the outer anthracene bond and 12.1 nA/T on the inside. The strengths of the local ring currents of the pyrenes and anthracenes in [**m21**] are shown in Figure 9.

5.2. Chemical Shieldings. The chemical shieldings are very sensitive to the strength of the ring currents. Especially, hydrogen shieldings are strongly affected by large ring currents. For benzene, the ^{13}C NMR shielding calculated at the BP86/def2-SVP level is 64.8 ppm and the ^{1}H NMR shielding is 24.0 ppm at the same level. The first series of molecules ([**m2**]−[**m6**]) has very small global ring currents, whereas all benzenes sustain local ring currents of about 9 nA/T yielding ^{1}H NMR shieldings of roughly 24 ppm. For [**m2**]−[**m6**], the ^{13}C NMR shieldings of the benzene carbons outside the main molecular ring are close to the value for a single benzene molecule, while the magnetic shieldings for the inner benzene carbons are about 10 ppm smaller. In [**m1**], the ^{13}C NMR shieldings are 103 ppm and for [**m2**]−[**m6**] the corresponding ^{13}C NMR shieldings are about 93 ppm. In [**m7**]−[**m21**], the carbons of the main molecular ring have ^{13}C NMR shieldings of about 80−90 ppm, where the carbons closer to the corner moieties have a 10 ppm larger shieldings than the carbons close to the edge group.

The ^{1}H NMR shieldings of the hydrogens in the edge moieties of molecules [**m7**]−[**m17**] possess the strongest dependence on the global ring−current strength. Consequently, the ^{1}H NMR shieldings vary in the same molecule between 8 and 57 ppm depending on the position. For [**m15**] with naphthalene moieties at the edges, the hydrogens in the naphthalene group inside the main ring have ^{1}H NMR shieldings of 48 ppm, whereas the naphthalene hydrogens on the outside have ^{1}H NMR shieldings of 8 and 17 ppm. The hydrogens in the corners of the main

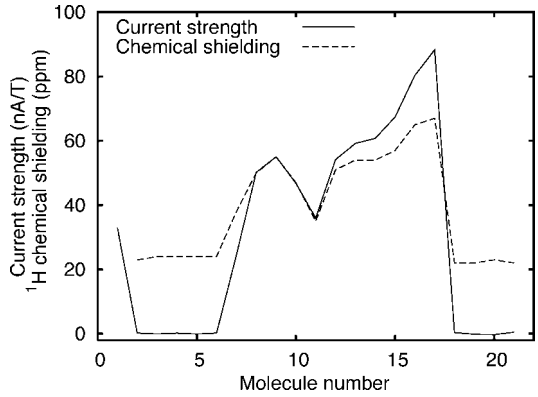

Figure 10. Comparison of the global ring current (in nA/T) and the ^{1}H NMR shieldings (in ppm) of the hydrogen in the corner group directed toward the center of the main ring.

TABLE 4: Static Polarizabilities and Polarizability Anisotropies (in 10^{-38} m^2 C^2/J) Calculated at the BP86/def2-SVP Level for the Investigated Molecules

	static polarizability in 10^{-38} m^2 C^2/J			
molecule	α_{xx}	α_{zz}	$(1/3)(\alpha_{xx}+\alpha_{yy}+\alpha_{zz})$	**A**
[**m1**]	0.071	0.013	0.052	0.059
[**m2**]	0.178	0.033	0.130	0.146
[**m3**]	0.484	0.065	0.344	0.418
[**m4**]	0.860	0.098	0.606	0.762
[**m5**]	1.273	0.131	0.893	1.142
[**m6**]	1.704	0.164	1.191	1.540
[**m7**]	0.679	0.057	0.472	0.622
[**m8**]	2.455	0.091	1.667	2.364
[**m9**]	5.960	0.123	4.014	5.836
[**m10**]	11.512	0.156	7.727	11.355
[**m11**]	19.182	0.189	12.851	18.993
[**m12**]	2.581	0.104	1.755	2.476
[**m13**]	2.557	0.118	1.744	2.439
[**m14**]	6.165	0.137	4.156	6.027
[**m15**]	6.398	0.151	4.316	6.247
[**m16**]	6.396	0.165	4.319	6.231
[**m17**]	6.358	0.178	4.298	6.180
[**m18**]	0.506	0.068	0.360	0.438
[**m19**]	0.918	0.101	0.646	0.817
[**m20**]	1.352	0.134	0.946	1.218
[**m21**]	1.240	0.128	0.869	1.112

ring of [**m15**], pointing toward the inside of the main ring, have the largest ^{1}H NMR shieldings of 57 ppm. For [**m17**] with two anthracene moieties at each edge, the smallest proton shieldings are 1.8 and 4.0 ppm while its largest ^{1}H NMR shielding is 67 ppm, which also is the largest proton shielding of the investigated molecules in this study. Figure 10 shows a clear correspondence between the ^{1}H NMR shielding of the hydrogen at the corner benzene pointing toward the center of the main molecular ring and the global ring−current strength.

5.3. Polarizabilities. The calculated static polarizabilities for the molecules labeled [**m1**]−[**m21**] are summarized in Table 4. The α_{xx} and α_{zz} components of the electric polarizability tensor are shown in Figures 11 and 12. The α_{xx} (α_{yy}) elements are much larger than α_{zz}, because the planar molecules are extended in the *xy* plane. The same holds for the polarizability anisotropies as for the α_{xx} components because α_{xx} is 1−3 orders of magnitude larger than α_{zz} for the studied molecules.

The calculations show that the polarizability increases monotonously from [**m1**] to [**m6**], whereas the global ring−current strength for [**m2**]−[**m6**] vanishes. The increase in the polarizability in the first series of molecules ([**m1**]−[**m6**]) is thus merely a size effect; the larger the molecular ring, the greater the polarizability.

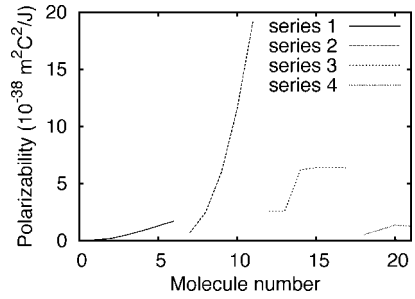

Figure 11. Calculated α_{xx} components of the static polarizabilities (in 10^{-38} m^2 C^2/J) for the studied molecules.

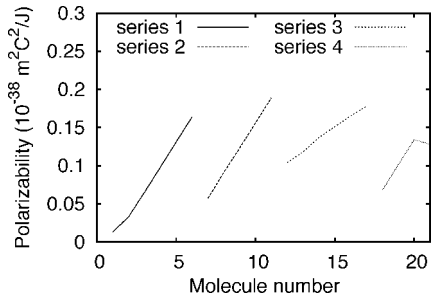

Figure 12. Calculated α_{zz} components of the static polarizabilities (in 10^{-38} m^2 C^2/J) for the studied molecules.

The polarizability of the second series of molecules ([**m7**]−[**m11**]) is significantly larger than for [**m1**]−[**m6**]. It can formally be separated into a ring−current contribution and a contribution originating from the size of the molecule. The ring−current contribution to the polarizability can be estimated by comparing the calculated polarizabilities for the molecules of the first series with the analogous ones in the second one. For example, the polarizability of [**m9**] can be considered to consist of a current contribution of 5.1×10^{-38} m^2 C^2/J if the molecular size contribution is assumed to be equal to the polarizability of [**m4**]. This is a reasonable assumption because [**m4**] and [**m9**] have the same size of the main molecular ring and the difference in the molecular structures appear only at the corner moieties. The estimated ring−current contribution to the polarizability dominates. Similar comparisons for the other molecules in the series show that the ring−current contribution to the polarizability increases with the size of the molecules, even though the current strength passes through a maximum for [**m9**]. A prerequisite of a large polarizability seems to be a significant ring−current susceptibility. However, for the molecules with nonvanishing ring currents in the main molecular ring, the ring−current strength does not obviously correlate with the polarizability.

The polarizability calculations on the third series of molecules show that they can be divided into two groups depending on the size of the main molecular ring. A comparison of the polarizabilities calculated for [**m9**] and [**m14**]−[**m17**] shows that the obtained polarizability is rather independent of the nature of the edge groups, whereas the length of the edge, thus the size of the main molecular ring, significantly affects the polarizability. The addition of pyrene-like corner groups yielding [**m18**]−[**m21**] destroys the formal aromatic character and leads to a drastic decrease of the polarizability. The ring currents of the main molecular ring of [**m18**]−[**m21**] also vanish.

6. Conclusions

Calculations of magnetically induced current densities with the GIMIC program[6] have been performed to elucidate the

current−pathway pattern for hydrocarbon nanorings with fused multiring structures. The calculations yielded rules to estimate the global and local ring−current strengths as well as the current pathways for the hexagon-shaped hydrocarbon nanorings. The strongest global ring currents were obtained for formally aromatic rings with phenalenyl moieties in the corners of the hexagon ([**m7**]−[**m17**]). The current strengths were enhanced by fused aromatic groups along the edges of the hexagon ring. The strongest ring current of 88 nA/T was obtained for [**m17**]. For the molecules sustaining strong currents in the main molecular ring, the fused aromatic edge groups do not sustain any local ring currents. Instead, the global ring current is split along the individual bonds of aromatic edge moieties fulfilling Kirchhoff's current law. In formally antiaromatic hydrocarbon nanorings, the fused benzene, naphthalene, anthracene, and pyrene moieties localize the ring current resulting in very weak global ring currents. Comparisons of calculated current densities and ^{1}H NMR shieldings yielded a clear correlation between the strength of the global ring currents and the hydrogen shielding of the inner hydrogens at the corner groups. For the studied molecules, the obtained ^{1}H NMR shieldings of the inner hydrogens and the global ring−current strengths are in the range of 22−67 ppm and 0−88 nA/T, respectively. The strong global ring current of 88 nA/T causes a ^{1}H NMR chemical shielding of 67 ppm, while in the same molecule, the smallest ^{1}H NMR chemical shielding is 1.8 ppm. The ^{13}C NMR shieldings were also found to be sensitive to the global ring−current strength, but they are though a less reliable measure of the current strength than the ^{1}H NMR shieldings. Calculations of the electric polarizabilities showed that the α_{xx} (and α_{yy}) elements of the polarizability tensor yield a merely qualitative measure of the global ring−current strengths, whereas α_{zz} depends mainly on the size of the nanoring.

Acknowledgment. This research has been supported by the Academy of Finland through its Centers of Excellence Programme 2006-2011 and from the Nordic Centre of Excellence in Computational Chemistry (NCoECC) (NordForsk 070253). CSC−the Finnish IT Center for Science is thanked for computer time. S.T. acknowledges Research Foundation of Orion Corporation and Alfred Kordelin Foundation for financial support. The research in Karlsruhe has been supported by the Deutsche Forschungsgemeinschaft (DFG) through the Center for Functional Nanostructures (CFN, Project No. C3.3). It has been further supported by a grant from the Ministry of Science, Research and the Arts of Baden-Württemberg (Az: 7713.14-300) and by the Fonds der Chemischen Industrie.

Supporting Information Available: The Cartesian coordinates of the molecular structures and the total energy of the molecules. This material is available free of charge via the Internet at http://pubs.acs.org.

References and Notes

(1) Datta, S. *Electronic Transport in Mesoscopic Systems*; Cambridge University Press: Cambridge, 1995.
(2) Busch, K.; von Freymann, G.; Lindén, S.; Mingaleev, S. F.; Tkeshellashvili, L.; Wegener, M. *Phys. Rep.* **2007**, *444*, 101–202.
(3) *Chem. Rev.* **2005**, *105*, 3433−3947.
(4) Chen, Z.; Heine, T.; Sundholm, D.; von Ragué Schleyer, P. *Aromaticity Indices from Magnetic Shieldings. In Quantum Chemical Calculation of Magnetic Resonance Properties*; Kaupp, M., Bühl, M., Malkin, V., Eds.; Wiley-VCH: Weinheim, Germany, 2004.
(5) Minkin, V. I.; Glukhovtsev, M. N.; Simkin, B. Y. *Aromaticity and Antiaromaticity−Electronic and Structural Aspects*; Wiley: New York, 1994.
(6) Jusélius, J.; Sundholm, D.; Gauss, J. *J. Chem. Phys.* **2004**, *121*, 3952–3963.
(7) Jusélius, J.; Sundholm, D. *Phys. Chem. Chem. Phys.* **1999**, *1*, 3429–3435.
(8) Jusélius, J.; Sundholm, D. *Phys. Chem. Chem. Phys.* **2000**, *2*, 2145–2151.
(9) Jusélius, J.; Sundholm, D. *J. Org. Chem.* **2000**, *65*, 5233–5237.
(10) Jusélius, J.; Sundholm, D. *Phys. Chem. Chem. Phys.* **2001**, *3*, 2433–2437.
(11) von Ragué Schleyer, P.; Maerker, C.; Dransfeld, A.; Jiao, H.; van Eikema Hommes, N. J. R. *J. Am. Chem. Soc.* **1996**, *118*, 6317–6318.
(12) Klod, S.; Kleinpeter, E. *J. Chem. Soc., Perkin Trans. 2* **2001**, 1893–1898.
(13) Heine, T.; Corminboeuf, C.; Grossmann, G.; Haeberlen, U. *Angew. Chem., Int. Ed.* **2006**, 7292–7295.
(14) Merino, G.; Vela, A.; Heine, T. *Chem. Rev.* **2005**, *105*, 3812–3841.
(15) Keith, T. A.; Bader, R. F. W. *Chem. Phys. Lett.* **1993**, *210*, 223–231.
(16) Zanasi, R.; Lazzeretti, P.; Malagoli, M.; Piccinini, F. *J. Chem. Phys.* **1995**, *102*, 7150–7151.
(17) Lazzeretti, P. *Prog. Nucl. Magn. Reson. Spectrosc.* **2000**, *36*, 1–88.
(18) Herges, R.; Geuenich, D. *J. Phys. Chem. A* **2001**, *105*, 3214–3220.
(19) Soncini, A.; Fowler, P. W.; Jenneskens, L. W. *Phys. Chem. Chem. Phys.* **2004**, *6*, 277–284.
(20) Havenith, R. W. A.; Engelberts, J. J.; Fowler, P. W.; Steiner, E.; van Lenthe, J.; Lazzeretti, P. *Phys. Chem. Chem. Phys.* **2004**, *6*, 289–294.
(21) London, F. *J. Phys. Radium* **1937**, *8*, 397–409.
(22) Hameka, H. *Mol. Phys.* **1958**, *1*, 203–215.
(23) Ditchfield, R. *Mol. Phys.* **1974**, *27*, 789–807.
(24) Wolinski, K.; Hinton, J. F.; Pulay, P. *J. Am. Chem. Soc.* **1990**, *112*, 8251–8260.
(25) Epstein, S. T. *J. Chem. Phys.* **1973**, *58*, 1592–1595.
(26) Lin, Y. C.; Jusélius, J.; Sundholm, D.; Gauss, J. *J. Chem. Phys.* **2005**, *122*, 214308.
(27) Lin, Y. C.; Sundholm, D.; Jus'elius, J. *J. Chem. Theory Comput.* **2006**, *2*, 761–764.
(28) Lin, Y. C.; Sundholm, D.; Jusélius, J.; Cui, L. F.; Li, X.; Zhai, H. J.; Wang, L. S. *J. Phys. Chem. A* **2006**, *110*, 4244–4250.
(29) Johansson, M. P.; Jusélius, J. *Lett. Org. Chem.* **2005**, *2*, 469–474.
(30) Johansson, M. P.; Jusélius, J.; Sundholm, D. *Angew. Chem., Int. Ed.* **2005**, *44*, 1843–1846.
(31) Jusélius, J.; Sundholm, D. *Phys. Chem. Chem. Phys.* **2008**, *10*, 6630–6634.
(32) Benassi, R.; Lazzeretti, P.; Taddei, F. *J. Phys. Chem.* **1975**, *79*, 848–851.
(33) Fowler, P. W.; Soncini, A. *Chem. Phys. Lett.* **2004**, *383*, 507–511.
(34) Gauss, J.; Stanton, J. F. *Adv. Chem. Phys.* **2002**, *123*, 355–422.
(35) Bauernschmitt, R.; Ahlrichs, R. *Chem. Phys. Lett.* **1996**, *256*, 454–464.
(36) Bauernschmitt, R.; Ahlrichs, R. *J. Chem. Phys.* **1996**, *104*, 9047–9052.
(37) Furche, F. *J. Chem. Phys.* **2001**, *114*, 5982–5992.
(38) Furche, F.; Rappoport, D. Density functional methods for excited states: equilibrium structure and electronic spectra. In *Computational and Theoretical Chemistry*; Olivucci, M., Ed.; Computational Photochemistry, Vol. 16; Elsevier: Amsterdam, 2005; Chapter III.
(39) Ahlrichs, R.; Bär, M.; Häser, M.; Horn, H.; Kölmel, C. *Chem. Phys. Lett.* **1989**, *162*, 165–169, for current version: see http://www.turbomole.de.
(40) Vosko, S. H.; Wilk, L.; Nusair, M. *Can. J. Phys* **1980**, *58*, 1200–1211.
(41) Perdew, J. P. *Phys. Rev. B* **1986**, *33*, 8822–8824.
(42) Becke, A. D. *Phys. Rev. A* **1988**, *38*, 3098–3100.
(43) Eichkorn, K.; Treutler, O.; Öhm, H.; Häser, M.; Ahlrichs, R. *Chem. Phys. Lett.* **1995**, *242*, 652–660.
(44) Weigend, F.; Ahlrichs, R. *Phys. Chem. Chem. Phys.* **2005**, *7*, 3297–3305.
(45) Pulay, P.; Hinton, J. F.; Wolinski, K. In *Nuclear Magnetic Shieldings and Molecular Structure*; Tossell, J. A., Ed.; NATO ASI Series C, 386 Kluwer: Amsterdam, 1993.
(46) Soncini, A.; Fowler, P. W.; Lepetit, C.; Chauvin, R. *Phys. Chem. Chem. Phys.* **2008**, *10*, 957–964.

JP805086Q